ARTICLE

On-chip Spectrometer Formed by a Multi-stage Structure

Weiping Wang[1*]   Li Jin[2]   Shaoyu Zhao[1]   Zhipeng Hu[2]   Xiaoyan Hu[1]

1. Information Science Academy of China Electronics Technology Group Corporation, Beijing, 100086, China
2. 38th Institute of China Electronics Technology Group Corporation, Hefei, 230088, China

ARTICLE INFO	ABSTRACT
	With apparent size and weight advantages, on-chip spectrometer could be a good choice for the spectrum analysis application which has been widely used in numerous areas such as optical network performance monitoring, materials analysis and medical research. In order to realize the broadband and the high resolution simultaneously, we propose a new on-chip spectrometer structure, which is a two-stage structure. The coarse wavelength division is realized by the cascaded Mach-Zehnder interferometers, which is the first stage of the spectrometer. The output of the Mach-Zehnder interferometers are further dispersed by the second stage structure, which can be realized either by arrayed waveguide gratings or by digital Fourier transform spectrometer structure. We further implemented the thermo-optic modulation for the arrayed waveguide gratings to achieve a higher spectral resolution. The output channel wavelengths of the spectrometer are modulated by the embedded heater to obtain the first order derivative spectra of the input optical signal to obtain a 2nm resolution. With respect to the computer simulation and device characterization results, the 400nm spectral range and the nanoscale resolution have been demonstrated.

1. Introduction

The application of optical spectrometers ranges in many areas, such as biochemical sensing, food and drug testing, medical treatment and environmental monitoring [1-4]. However, due to the size, high power consumption and price, difficult for secondary development, the application of traditional spectrometers has been greatly limited. Compared to the traditional spectrometers, miniaturized spectrometers have the advantages of low cost, small volume, low power consumption and easy secondary development, which expands the application. Nevertheless, miniaturized

spectrometer which is usually based on discrete optical components, doesn't have high integration and flexibility. As more and more high to the requirement of portability, further miniaturization and integration have become a trend of spectrometer. On-chip spectrometers, with apparent Size, Weight, and Power (SWaP) advantages, have unprecedented impact on applications ranging from unmanned devices to intelligent platform. During the last few years, on-chip spectrometers have become an enormously active area, resulting in significant progress [5-12]. Among the methods to realize on-chip spectrometers, silicon photonics offers an approach to realize an integrated and cheap spectroscopic system because

Corresponding Author:
Weiping Wang,
Information Science Academy of China Electronics Technology Group Corporation, Beijing, 100086, China;
Email: li.jin@cumec.cn

of its mature processing and integration [13]. The silicon-based on-chip spectrometer can be realized by either dispersive components, or interferometers. Dispersive components like Echelle diffraction gratings (or planar concave grating) and arrayed waveguide gratings(AWG) can achieve a high resolution, but suffer serious SNR penalties when designed for high spectral resolution, which precludes high performance spectrometers with a large bandwidth. The spectrometer based on interference can obtain a large bandwidth with a high SNR benefiting from the multiplex advantage. However, compared to the dispersive components, it's difficult to realize a high resolution. In application, compact, broadband, and high-resolution spectrometers are appealing for sensing application.

In this work, we propose and experimentally demonstrate a novel spectrometer architecture. The spectrometer is realized by a multi-stage structure, which combines the high resolution advantage of dispersive components and the broadband advantage of interference structure. We further implemented the thermos-optic modulation to achieve a higher spectral resolution. Compared with other existing on-chip spectrometers, the multi-stage waveguide spectrometer can achieve both a broadband spectral range and a relatively high resolution.

2. Methods

In this work, there are two methods to realize the spectrometer. As shown in Figure 1, the spectrometer is a multi-stage structure. The first stage of the structure is a cascaded Mach-Zehnder Interferometer (MZI) structure based coarse wavelength division de-multiplexer to separate the signal of 1150-1550 nm into four channels with a channel spacing of 100 nm. Then, the second stage can be realized by two ways, one way is the AWG structures, and the other is digital Fourier transform structures. The signal in each of the four outputs of the cascaded MZIs can be individually dispersed into 8 channels further with a channel spacing of 12.5 nm by the AWG structures. Finally, the output channel wavelengths of AWGs are modulated (with a wavelength shift 2 nm) by the embedded heater to obtain the first order derivative spectra of the input optical signal. In order to improve the resolution, a digital Fourier transform (dFT) spectrometer can been also developed as the alternative for the second stage, which is formed by a reconfigurable MZI (more details in Discussion part). The two stage structure with a cascaded MZI and AWGs will be firstly introduced as follows.
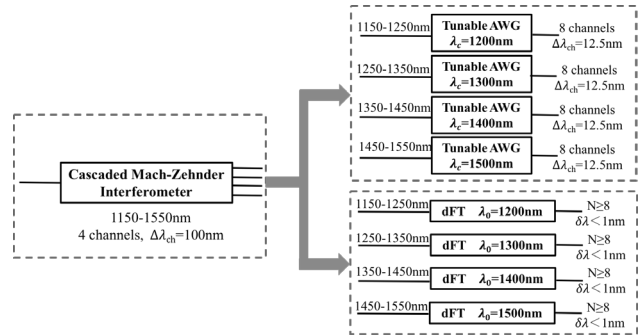

Figure 1. On-chip spectrometer principle block diagram

2.1 The Cascaded Mach-Zehnder Interferometer

The cascaded MZI shown in Figure 2 was employed for the first stage of the spectrometer and was used to disperse the 1150-1550 nm signal into four channels with a channel spacing of 100 nm. By cascading multiple MZIs, the pass band can be engineered while keeping the device quite compact [14]. The MZI is constructed by connecting two directional couplers with an optical delay line. The free spectral range ($\Delta\lambda$) of the individual MZI is inversely proportional to the delay length (ΔL)

$$\Delta\lambda = \frac{\lambda_c^2}{n_g * \Delta L} \qquad (1)$$

Where λ_c is the center wavelength, ΔL is the physical path length difference between longer and shorter arm of the MZI and n_g is group index of the designed waveguide which is defined as:

$$n_g = n_e - \lambda \frac{dn_e}{d\lambda} \qquad (2)$$

Where n_e is the effective index. The operating wavelength of the cascaded structure is centered at 1350 nm and each MZI at this stage is designed for a free spectral range ($\Delta\lambda$) of 200 nm and 400 nm, respectively. The ΔL was selected to be $2 \times 1.33 \mu m$ and $2 \times 0.67 \mu m$ for first and second MZI structures, respectively. The performance of this MZI cascaded structure was studied by the 2.5D FDTD method. As shown in Figure 3, according to the simulation results, the peak transmission efficiency of the MZI structure was determined to be ranged from $55 - 65\%$ (-2.5 dB) and the bandwidth for each channel were 100 nm which were sufficient for our application.
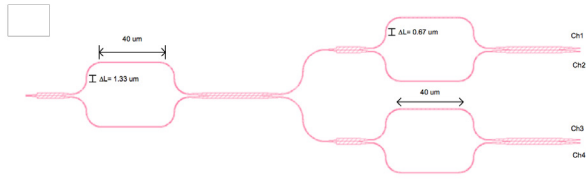
Figure 2. Schematic of the cascaded MZI
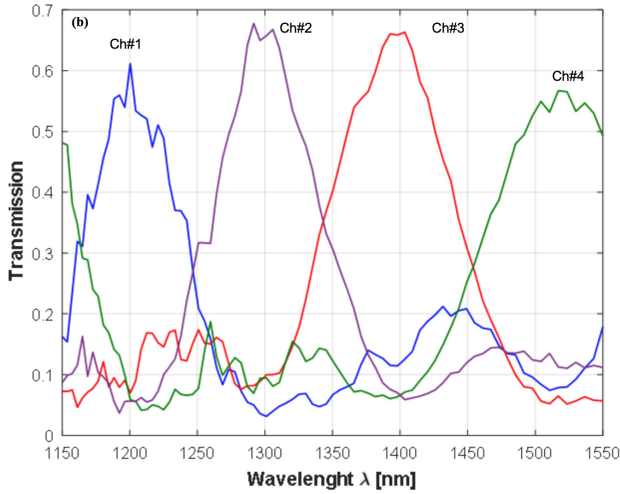
Figure 3. Simulation results of the cascaded MZI

2.2 Arrayed Waveguide Grating

An AWG consists of two star-couplers and an array of waveguides with constant successive increment of length (ΔL), shown as Figure 4. The input and output apertures of the phased array are in the Rowland circle configuration [15] such that the image plane follows a circle with radius f. The working principle of an AWG is based on the optical phased array, which has identical elements and constant phase difference between successive elements. The light enters into input star-coupler and diverges. This diverging light beam is then coupled in an array of waveguides and propagates through these waveguides to a second star-coupler. Hence, the AWG equation can be written as:

$$n_a \cdot \Delta L + n_s da \sin\theta = m\lambda \qquad (3)$$

in which n_s and n_a are the effective index of the slab and arrayed waveguides respectively, m is the diffraction order, and d_a is the pitch of adjacent arrayed waveguides.
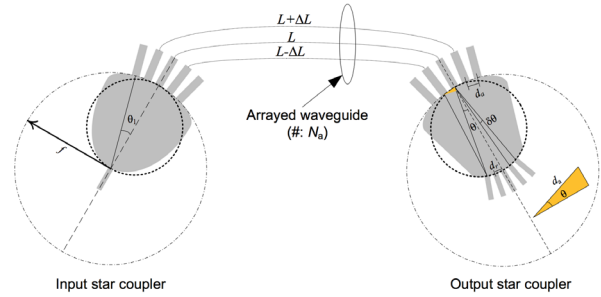
There are three major equations in the AWG design, which describe the design parameters and the relationship of the center wavelength (λ_c), free spectral range ($\Delta\lambda$) and angular dispersion ($d\theta/d\lambda$):

$$\lambda_c = \frac{n_a \cdot \Delta L}{m} \qquad (4)$$

$$\frac{d\theta}{d\lambda} \approx \frac{mn_g}{n_s n_a d_a} \qquad (5)$$

$$\Delta\lambda = \frac{\lambda_c \cdot n_a}{mn_g} \qquad (6)$$

in which n_g is the group index of the arrayed waveguides.

Figure 4. Illustration of AWG structure [15]

Although the above equations show that there are many degrees of freedom for the AWG design, its design parameters are also limited by the design rule of specific fabrication process. For example, the effective index n_a is dependent on the width (w) and height (h) of the waveguide but the h in the actual device fabrication is limited to be the thickness of the Si layer in the SOI wafer. In this work, the w and h of the arrayed waveguide were fixed to be 0.5 μm and 220 nm, respectively.

In this work, the design was based on the modeling result of 2.5D FDTD method by Lumerical. We have designed and simulate 4 AWGs with λ_c =1200nm, 1300nm, 1400nm and 1500nm, each AWG has a free spectral range of 100nm and a channel space of 12.5nm. One of the computer simulation results for AWG structures (l_c of 1500 nm) were shown in the Figure 5. The free spectral range and channel spacing of the AWG structure (λ_c of 1500 nm) was determined to 100 nm and 12.5 nm. The transmission efficiency for all channels was determined to be > 20% (-6 dB). Hence, the total loss of this on-chip spectrometer design was determined to be 14.5 dB including a 2.5 dB loss from MZI, 6 dB loss from AWG structure and 2×3dB loss from the input and output coupling.
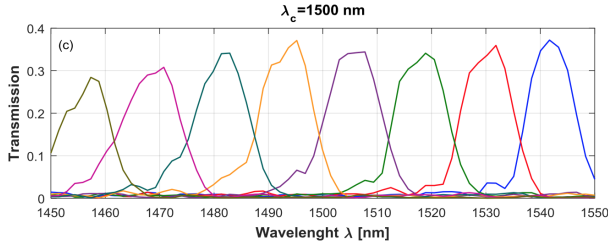
Figure 5. The modeling results of the AWG structure with designed λ_c of 1500 nm

2.3 Thermo-optic Modulation

In order to improve the spectral resolution, the spectrum derivation was performed by introducing the thermo-optic modulation. Derivative spectroscopy utilizes the derivatives of the absorption spectrum data for qualitative and quantification chemical analysis. The derivative spectroscopy technology was first introduced in 1950s by A. Giese et al [16] to measure the low intensity bands overlapped by bands of higher intensity in the absorption spectra. Our design has leveraged the tunable AWG structures for the spectrum derivation. An embedded heater structures were added on top of these AWG structures for the refractive index (n) modulation by the thermo-optic (TO) effect:

$$\frac{dn}{dT} = C_T \tag{7}$$

where C_T is the TO coefficient and is determined to be $+1.84\times10^{-4}$/K and 10^{-5}/K for the silicon and silicon dioxide, respectively. Hence, the central wavelength shift ($\Delta\lambda_c$) arising from the change of a temperature (ΔT) due to the TO effect can be calculated by [17]:

$$\Delta\lambda_c = \frac{\Delta n_a}{n_g}\lambda_c = \frac{\lambda_c}{n_g}(\frac{\partial n_a}{\partial n_{si}}\Delta n_{si} + \frac{\partial n_a}{\partial n_{sio_2}}\Delta n_{sio_2}) \tag{8}$$

where n_{si} and n_{sio2} denote the refractive index of silicon and silicon dioxide, respectively. When the center wavelength λ_c is shifted, the transmission spectra at State 1 and State 2 are recorded. Then, the first-order derivative spectrum of the input signal can be directly obtained as $I' = (I_{state1} - I_{state2})/dl$.

2.4 Fabrication

The fabrication process of the on-chip spectrometer is shown in Figure 6. The device was fabricated on a silicon on insulator (SOI) wafer with 220 nm silicon and 2 μm buried oxide. The embedded heater structure for the on-chip spectrometer has also been added. The unit size of

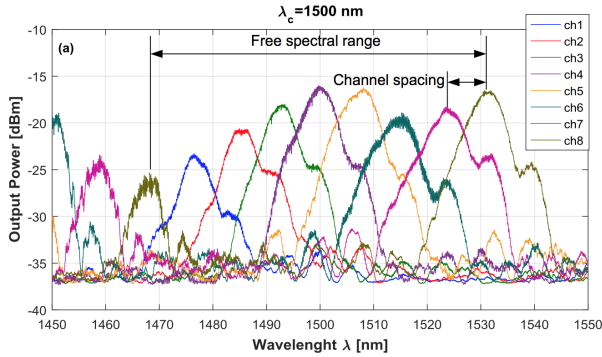the on-chip spectrometer is 3mm×3mm.
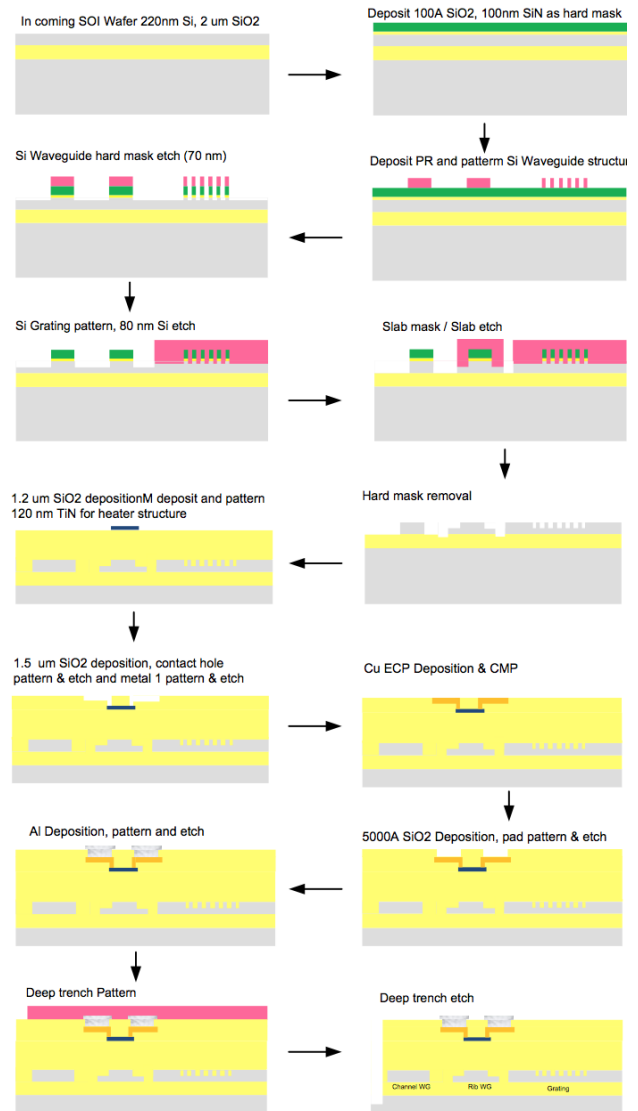
**Figure 6.** The passive silicon photonic fabrication process

3. Results

The performance of the device was characterized by injecting 1mW (0dBm) optical signal with a λ ranging from 1440 to 1640 nm into the spectrometer using a tunable laser, the measurement results for λ_c of 1500 nm were shown in Figure 7. As shown in the Figure 7, the free spectral range and channel spacing of the AWG with a λ_c of 1500 nm were determined to be 65 nm and 8 nm, respectively, which were less than the designed values of 100 nm and 12.5 nm, respectively. According to equation (5) and (6), these reductions indicated that the effective group index n_g of the fabricated device is smaller than that of the computer simulation. Besides, the loss of the spectrometer was determined to be ~16 dB which was higher

than the 14.5 dB from the computer simulation. These performance degradations were generally due to fabrication tolerance and imperfection for device fabrication process.

Figure 7. The measurement result of the on-chip spectrometer: the spectra at the 8 output channels of the AWG structure with λ_c =1500 nm

By applying a voltage ranging from 0 to 20 V across the embedded heater structure, a change of λ_c from 0 to 0.8 nm was observed and this was sufficient for spectrum derivation, shown as Figure 8.
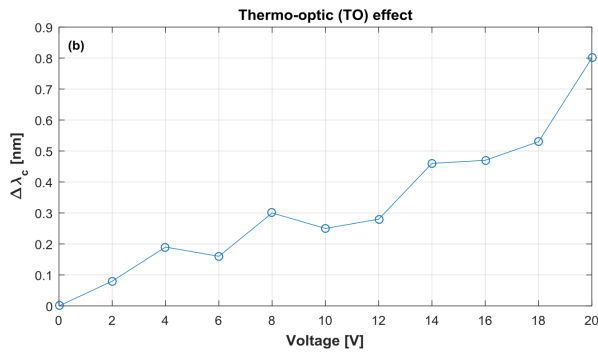
Figure 8. The measurement result of the thermo-optic effect for λ_c modulation.

4. Discussion

Compared with dispersive spectrometers, Fourier transform spectrometers benefits the advantage of signal-to-noise ratio. Generally, on-chip Fourier transform spectrometers mainly rely on thermo-optic or electro-optic modulation to change the optical path length in a waveguide [18]. These effects can produce minute refractive index modifications, however, resulting in large device size and constraining the practically attainable spectral resolution to tens of cm⁻¹ in wave number. The digital Fourier transform spectrometer can overcome this limitation [19]. As shown in Figure 9(a), the spectrometer is a reconfigurable MZI. Each arm consists of j/2 cascaded sets of optical switches connected by waveguides of varying lengths, where j is an even integer (j=2(K+1), k ∈ [1, K]). When light propagates through the reference paths (marked with black color) in both MZI arms, the MZI is balanced with zero optical path length difference between the two arms. Lengths of the waveguide paths in red differ from the reference paths by a power of two times ΔL. Each permutation of the switches thus corresponds to a unique optical path length difference between the arms, covering 0 to (2j-1)·n_g·ΔL with a step size of n_g·ΔL, where n_g represents the waveguide group index. The number of spectral channels, defined by the distinctive optical states the device furnishes, is:

$$N = 2^j \tag{9}$$

and the spectral resolution is given following the Rayleigh criterion [19, 20]:

$$\delta\lambda = \frac{\lambda^2}{(2^j - 1)\cdot n_g \Delta L} \approx \frac{1}{2^j}\cdot\frac{\lambda^2}{n_g \Delta L} \tag{10}$$

where l denotes the center wavelength. A dFT spectrometer has been designed with N=8, and the layout is shown as Figure 9(b). Unlike the dispersive spectrometer, both the spectral channel count and resolution of the dFT spectrometer scale exponentially with the number of cascaded switch stages. This unique exponential scaling behavior allows high-resolution spectroscopy with a radically simplified device architecture. Then, compared to thermo-optic or electro-optic-based index modulation, direct modification of the waveguide path offers much larger optical length path tuning, enabling superior spectral resolution within a compact device. The device also benefits from the multiplex advantage to ensure significantly enhanced signal-to-noise ratio over the dispersive devices. Moreover, the spectrometer only requires a single-element photodetector rather than a linear array, which further reduces system complexity and cost. Thus, the dFT structure is a good alternative to replace AWGs, which is also the focus of the future research.
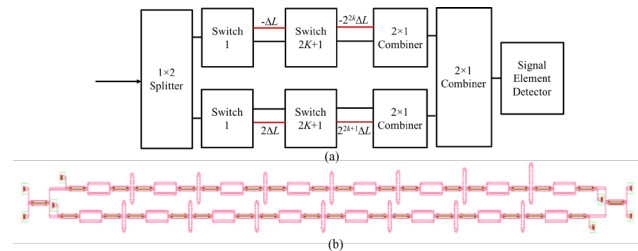
Figure 9. (a) Block diagram illustrating the generic structure of a dFT spectrometer. (b)The mask layout of the dFT structure with j/2=8

5. Conclusions

A multi-stage on-chip spectrometer has been proposed and demonstrated. The spectrometer was designed by a 2-stage waveguide structure with a cascaded MZI and AWGs, which can realize a spectral range of 400 nm and a spectrum resolution of 2 nm for performing spectrum derivation. From the characterization results, we found that the device performances, including free spectral range, channel spacing and optical loss, were slightly poorer than the simulation results. This implies that the fabrication tolerance and imperfection are larger than the disclosed design rule from the foundry. A dFT spectrometer has been also discussed to be used as the second stage of the on-chip spectrometer, which can help improve the resolution greatly. Compared with other existing on-chip spectrometer, the cascaded waveguide spectrometer can achieve both a broadband spectral range and a relatively high resolution, which makes it potential in sensing application.

Acknowledgments

References

[1] J. T. Kindt, M. S. Luchansky, A. J. Qavi, et al. Subpicogram per milliliter detection of interleukins using silicon photonic microring resonators and an enzymatic signal enhancement strategy [J]. Anal. Chem., 8(22): 10653-10657.
DOI: 10.1021/ac402972d

[2] E. Ryckeboer, R. Bockstaele, M. Vanslembrouck, et al. Glucose sensing by waveguide-based absorption spectroscopy on a silicon chip [J]. Biomed. Opt. Express, 5(5): 1636–1648.
DOI: 10.1364/BOE.5.001636

[3] Y. Chen, H. Lin, J. Hu, et al. Heterogeneously Integrated Silicon Photonics for the Mid-Infrared and Spectroscopic Sensing [J]. ACS Nano, 5(7): 6955–6961.
DOI: 10.1021/nn501765k

[4] Tseng V F G, Xie H.. Simultaneous piston position and tilt angle sensing for large vertical displacement micromirrors by frequency detection inductive sensing [J]. Applied Physics Letters, 107(21): 214102.
DOI: 10.1063/1.4936375

[5] Noel H. Wan, Fan Meng, Tim Schröder, Ren-Jye Shiue, et al. High-resolution optical spectroscopy using multimode interference in a compact tapered fibre [J]. Nat. Commun., 6: 7762.
DOI: 10.1038/ncomms8762

[6] Redding, B., Liew, S. F., Bromberg, Y., et al. Evanescently coupled multimode spiral spectrometer [J]. Optica, 3: 956–962.
DOI: 10.1364/OPTICA.3.000956

[7] Subramanian, A. Z. et al. Silicon and silicon nitride photonic circuits for spectroscopic sensing on-a-chip [J]. Photonics Res., 3: B47–B59.
DOI: 10.1364/PRJ.3.000B47

[8] Podmore H, Scott A, Cheben P, et al. Demonstration of a compressive-sensing Fourier-transform on-chip spectrometer [J]. Opt. Lett., 42(7): 1440–1443.
DOI: 10.1364/OL.42.001440

[9] Akca, B. I.. Design of a compact and ultrahigh-resolution Fourier-transform spectrometer [J]. Opt. Express, 25(2): 1487–1494.
DOI: 10.1364/OE.25.001487

[10] Herrero-Bermello A, Velasco AV, Podmore H, et al. Temperature dependence mitigation in stationary Fourier-transform on-chip spectrometers [J]. Opt. Lett., 42(11): 2239–2242.
DOI: 10.1364/OL.42.002239

[11] Sabry, Y. M., Khalil, D., Bourouina, T.. Monolithic silicon-micromachined free-space optical interferometers on chip [J]. Laser Photonics Rev., 9(1): 1–24.
DOI: 10.1002/lpor.201400069

[12] Erfan M, Sabry YM, Sakr M, et al. On-Chip Micro-Electro-Mechanical System Fourier Transform Infrared (MEMS FT-IR) Spectrometer-Based Gas Sensing [J]. Appl. Spectrosc., 70(5): 897–904.
DOI: 10.1177/0003702816638295

[13] A. E.-J. Lim, Junfeng Song, Qing Fang, et al. Review of Silicon Photonics Foundry Efforts [J]. IEEE J. Sel. Top. Quantum Electron., 20(4): 405–416.
DOI: 10.1109/JSTQE.2013.2293274

[14] Dwivedi, S., et al. Coarse wavelength division multiplexer on silicon-on-insulator for 100 GbE [R]. in Group IV Photonics (GFP) IEEE 12th International Conference, 2015.
DOI: 10.1109/Group4.2015.7305928

[15] Seyringer, D., et al. Design and simulation of 20-channel 50-GHz Si3N4-based arrayed waveguide grating applying AWG-parameters tool [R]. in SPIE OPTO. 2017: SPIE.
DOI: 10.1117/12.2249675

[16] Giese, A.T. and C.S. French. The analysis of overlapping spectral absorption bands by derivative spectrophotometry [J]. Applied spectroscopy, 9(2): 78-96.
DOI: 10.1366/000370255774634089

[17] Yang, Y., et al. Thermo-Optically Tunable Silicon AWG With Above 600 GHz Channel Tunability [J].

IEEE Photonics Technology Letters, 27(22): 2351-2354.
DOI: 10.1109/LPT.2015.2464073

[18] Li, J., Lu, D.-f. & Qi, Z.-m. Miniature Fourier transform spectrometer based on wavelength dependence of half-wave voltage of a LiNbO3 waveguide interferometer [J]. Opt. Lett., 39(13): 3923-3926.
DOI: 10.1364/OL.39.003923

[19] Kita, D. et al. On-chip infrared spectroscopic sensing: redefining the benefits of scaling [J]. IEEE Journal of Selected Topics in Quantum Electronics, 23: 5900110.
DOI: 10.1109/PIERS.2016.7734993

[20] Lin Hongtao, Luo Zhengqian, Gu Tian, et al. Mid-infrared integrated photonics on silicon: a perspective [J]. Nanophotonics, 7: 393-420.
DOI: 10.1515/nanoph-2017-0085